Supplementary Materials for

Quantum squeezing skyrmions

Zijian Lyu[1], Jingze Li[1], and Yunquan Liu[1,2,3*]

[1] *State Key Laboratory for Mesoscopic Physics and Frontiers Science Center for Nano-optoelectronics, School of Physics, Peking University, Beijing, 100871, China*
[2] *Collaborative Innovation Center of Extreme Optics, Shanxi University, Taiyuan, 030006, China*
[3] *Peking University Yangtze Delta Institute of Optoelectronics, Nantong, Jiangsu, 226010, China*

[*]Correspondence: Yunquan.Liu@pku.edu.cn

Contents

1 SU(2) and SU(1,1) geometrical frameworks for optical skyrmions **1**
2 Off-axis analysing vortex for phase reconstruction **2**
3 Spatial-mode selection in the two-BBO system **5**
3.1 High-gain mode generation in BBO1 5
3.2 Propagation and mode-dependent amplification in BBO2 5
3.3 Two-crystal high-gain output 6
References **7**

1. SU(2) and SU(1,1) geometrical frameworks for optical skyrmions

Table 1: **Comparison between conventional $\mathrm{SU}(2)$ optical skyrmions and $\mathrm{SU}(1,1)$ quantum squeezing skyrmions [1, 2].** Conventional optical skyrmions are encoded in first-order coherence and inherit the compact $\mathrm{SU}(2)$ geometry of the Bloch–Poincaré sphere [3, 4]. Quantum squeezing skyrmions are encoded in anomalous second-order coherence. Their native $\mathrm{SU}(1,1)$ covariance coordinates occupy a non-compact hyperbolic manifold, from which a compact covariance texture supporting an integer skyrmion charge is constructed.

Property	**Conventional $\mathrm{SU}(2)$ optical skyrmion**	**$\mathrm{SU}(1,1)$ quantum squeezing skyrmion**
Basic variables	Jones spinor $(\hat{a}_0, \hat{a}_1)^{\mathrm{T}}$	Nambu spinor $(\hat{a}_0, \hat{a}_1^\dagger)^{\mathrm{T}}$
Basic matrix	First-order coherence matrix $\Gamma = \frac{1}{2}(S_0 I + S_1\sigma_x + S_2\sigma_y + S_3\sigma_z)$	Symmetrically ordered Nambu covariance matrix $\mathcal{G} = \frac{1}{2}(K_0 I + K_1\sigma_x + K_2\sigma_y + K_3\sigma_z)$
Key correlation	First-order coherence $C = \langle \hat{a}_0^\dagger \hat{a}_1 \rangle$	Anomalous pair coherence $M = \langle \hat{a}_0 \hat{a}_1 \rangle$
Transverse components	$S_1 = 2\,\mathrm{Re}\,C, \qquad S_2 = 2\,\mathrm{Im}\,C$	$K_1 = 2\,\mathrm{Re}\,M, \qquad K_2 = 2\,\mathrm{Im}\,M$
Population imbalance	$S_3 = N_0 - N_1$	$K_3 = N_0 - N_1$
Scalar component	Total modal population $S_0 = N_0 + N_1$	Total symmetrized fluctuation $K_0 = N_0 + N_1 + 1$
		The additional unity originates from the symmetrically ordered vacuum contribution.
Generators	$\hat{J}_1 = \frac{\hat{a}_0^\dagger \hat{a}_1 + \hat{a}_1^\dagger \hat{a}_0}{2}$, $\hat{J}_2 = \frac{\hat{a}_0^\dagger \hat{a}_1 - \hat{a}_1^\dagger \hat{a}_0}{2i}$, $\hat{J}_3 = \frac{\hat{N}_0 - \hat{N}_1}{2}$	$\hat{L}_1 = \frac{\hat{a}_0^\dagger \hat{a}_1^\dagger + \hat{a}_0 \hat{a}_1}{2}$, $\hat{L}_2 = \frac{\hat{a}_0 \hat{a}_1 - \hat{a}_0^\dagger \hat{a}_1^\dagger}{2i}$, $\hat{L}_3 = \frac{\hat{N}_0 + \hat{N}_1 + 1}{2}$
Components versus generators	$(S_1, S_2, S_3) = 2\big(\langle \hat{J}_1 \rangle, \langle \hat{J}_2 \rangle, \langle \hat{J}_3 \rangle\big)$	$(K_1, K_2, K_0) = 2\big(\langle \hat{L}_1 \rangle, \langle \hat{L}_2 \rangle, \langle \hat{L}_3 \rangle\big)$
		Here K_3 is a population-imbalance coordinate rather than an additional $\mathrm{SU}(1,1)$ generator.
Commutation relations	$[\hat{J}_i, \hat{J}_j] = i\epsilon_{ijk}\hat{J}_k$	$[\hat{L}_i, \hat{L}_j] = i\epsilon_{ijk}\eta^{k\ell}\hat{L}_\ell, \qquad \eta = \mathrm{diag}(-1,-1,1)$
Native metric	Euclidean metric δ_{ij}	Lorentz metric acting on (K_0, K_1, K_2) $\eta_{\mathrm{L}} = \mathrm{diag}(1,-1,-1)$
Geometrical constraint	The normalized Stokes vector satisfies $\|\boldsymbol{s}\|^2 = 1$	For an ideal two-mode squeezed vacuum $K_0^2 - K_1^2 - K_2^2 = 1$

Continued on the next page

Supplementary Table 1 (continued)

Property	**Conventional $\mathrm{SU}(2)$ optical skyrmion**	**$\mathrm{SU}(1,1)$ quantum squeezing skyrmion**
Native geometrical space	Compact Bloch–Poincaré sphere	Upper sheet of the non-compact two-sheet hyperboloid
	S^2	H^2
Native topological classification	$\pi_2(S^2) = \mathbb{Z}$	$\pi_2(H^2) = 0$
Correlation order carrying the texture	First-order coherence	Anomalous second-order coherence
Texture vector	Normalized local Stokes vector	Normalized local covariance vector
	$\boldsymbol{s}(\boldsymbol{r}) = \dfrac{\boldsymbol{S}(\boldsymbol{r})}{\|\boldsymbol{S}(\boldsymbol{r})\|}$	$\boldsymbol{n}(\boldsymbol{r}) = \dfrac{\boldsymbol{d}(\boldsymbol{r})}{\|\boldsymbol{d}(\boldsymbol{r})\|}, \quad \boldsymbol{d}(\boldsymbol{r}) = \big(K_1(\boldsymbol{r}), K_2(\boldsymbol{r}), K_3(\boldsymbol{r})\big)^{\mathrm{T}}$
Topological classification	$\pi_2(S^2) = \mathbb{Z}$	$\pi_2(S^2) = \mathbb{Z}$
Topological charge	$Q = \dfrac{1}{4\pi}\displaystyle\int \boldsymbol{s}\cdot(\partial_x\boldsymbol{s}\times\partial_y\boldsymbol{s})\,dx\,dy$	$Q = \dfrac{1}{4\pi}\displaystyle\int \boldsymbol{n}\cdot(\partial_x\boldsymbol{n}\times\partial_y\boldsymbol{n})\,dx\,dy$
Typical measurement	Polarization projection, mode interference and Stokes tomography	Phase-sensitive optical parametric amplification, quadrature scanning and covariance tomography

Sign and metric conventions. The metric $\eta = \mathrm{diag}(-1,-1,1)$ in the compact expression for the $\mathrm{SU}(1,1)$ commutation relations is ordered according to (L_1, L_2, L_3), with L_3 as the timelike generator. In contrast, $\eta_{\mathrm{L}} = \mathrm{diag}(1,-1,-1)$ is ordered according to the Lorentzian covariance coordinates (K_0, K_1, K_2).

2. Off-axis analysing vortex for phase reconstruction

The phase-sensitive optical parametric amplifier (OPA) measures the relative phase between the anomalous pair coherence of the incident field and the pump field. In the present experiment, the spatially dependent pair coherence can be written as

$$M(\boldsymbol{r}) = |M(\boldsymbol{r})|\exp[i\delta_M(\boldsymbol{r})]\,, \qquad \delta_M(\boldsymbol{r}) = \ell\varphi + \varphi_0, \tag{1}$$

where $\boldsymbol{r} = (r,\varphi)$, ℓ is the azimuthal winding number, and φ_0 is a spatially uniform phase offset. Correspondingly, the two transverse covariance components defined in the main text satisfy

$$K_1(\boldsymbol{r}) + iK_2(\boldsymbol{r}) = 2|M(\boldsymbol{r})|\exp[i(\ell\varphi + \varphi_0)]\,. \tag{2}$$

If the pump of the analysing OPA carries an OAM charge ℓ_a, its spatially varying phase must also be included in the phase-sensitive OPA transformation. Denoting the analysing-pump phase by $\Phi_a(\boldsymbol{r})$, the phase-dependent output photon-number distribution can be expressed as

$$n_{\mathrm{tot}}(\boldsymbol{r};\delta) = n_{\mathrm{bg}}(\boldsymbol{r}) + A(\boldsymbol{r})\cos[\delta - \delta_{\mathrm{rel}}(\boldsymbol{r})]\,, \tag{3}$$

where δ is the globally scanned pump–signal phase, $n_{\mathrm{bg}}(\boldsymbol{r})$ is the phase-insensitive background, and $A(\boldsymbol{r})$ is the local phase-sensitive modulation amplitude. The phase extracted from the OPA response is

$$\delta_{\mathrm{rel}}(\boldsymbol{r}) = \delta_M(\boldsymbol{r}) - \Phi_a(\boldsymbol{r}). \tag{4}$$

Thus, the phase-sensitive OPA measures the phase of the anomalous pair coherence relative to the local phase of the analysing pump.

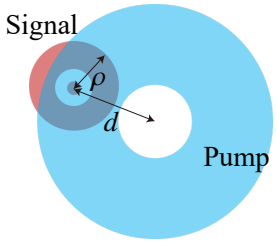
For perfectly concentric signal and analysing-pump vortices, the analysing-pump phase is

$$\Phi_a(\boldsymbol{r}) = \ell_a \varphi. \tag{5}$$

Substitution into Eq. (4) gives

$$\delta_{\mathrm{rel}}(\boldsymbol{r}) = (\ell - \ell_a)\varphi + \varphi_0. \tag{6}$$

For equal winding numbers, $\ell_a = \ell$, the two azimuthal phase dependences cancel and the measured relative phase reduces to the spatially uniform offset φ_0. Consequently, no phase-dependent rotation of the bright lobe occurs, and the winding of $M(\boldsymbol{r})$ cannot be recovered from the relative-phase map. To prevent this cancellation, we experimentally



S1. Schematic of the displacement between the pump phase singularity and signal center at the OPA. Here, ρ is the signal reconstruction radius and d is the singularity displacement. For $d > \rho$, the pump phase contributes zero net winding and does not cancel the signal winding.

adjust the transverse position of the spiral phase plate, thereby controlling the relative displacement between the analysing-pump phase singularity and the centre of the signal texture at the OPA, as schematically illustrated in Fig. S1.

When the analysing-pump singularity is displaced from the signal centre by a transverse vector $\boldsymbol{d} = d(\cos\varphi_d, \sin\varphi_d)$, its phase in signal-centred coordinates becomes

$$\Phi_a(\boldsymbol{r}) = \ell_a \arg\left(re^{i\varphi} - de^{i\varphi_d}\right). \tag{7}$$

The relative phase measured by the phase-sensitive OPA is therefore

$$\delta_{\mathrm{rel}}(r,\varphi) = \ell\varphi + \varphi_0 - \ell_a \arg\left(re^{i\varphi} - de^{i\varphi_d}\right). \tag{8}$$

Without loss of generality, the displacement direction can be chosen as the x axis, such that $\varphi_d = 0$. Equation (8) then reduces to

$$\delta_{\mathrm{rel}}(r,\varphi) = \ell\varphi + \varphi_0 - \ell_a \arg\left(re^{i\varphi} - d\right). \tag{9}$$

The corresponding local azimuthal phase gradient is

$$\frac{\partial\delta_{\mathrm{rel}}}{\partial\varphi} = \ell - \ell_a \frac{r^2 - rd\cos\varphi}{r^2 + d^2 - 2rd\cos\varphi}. \tag{10}$$

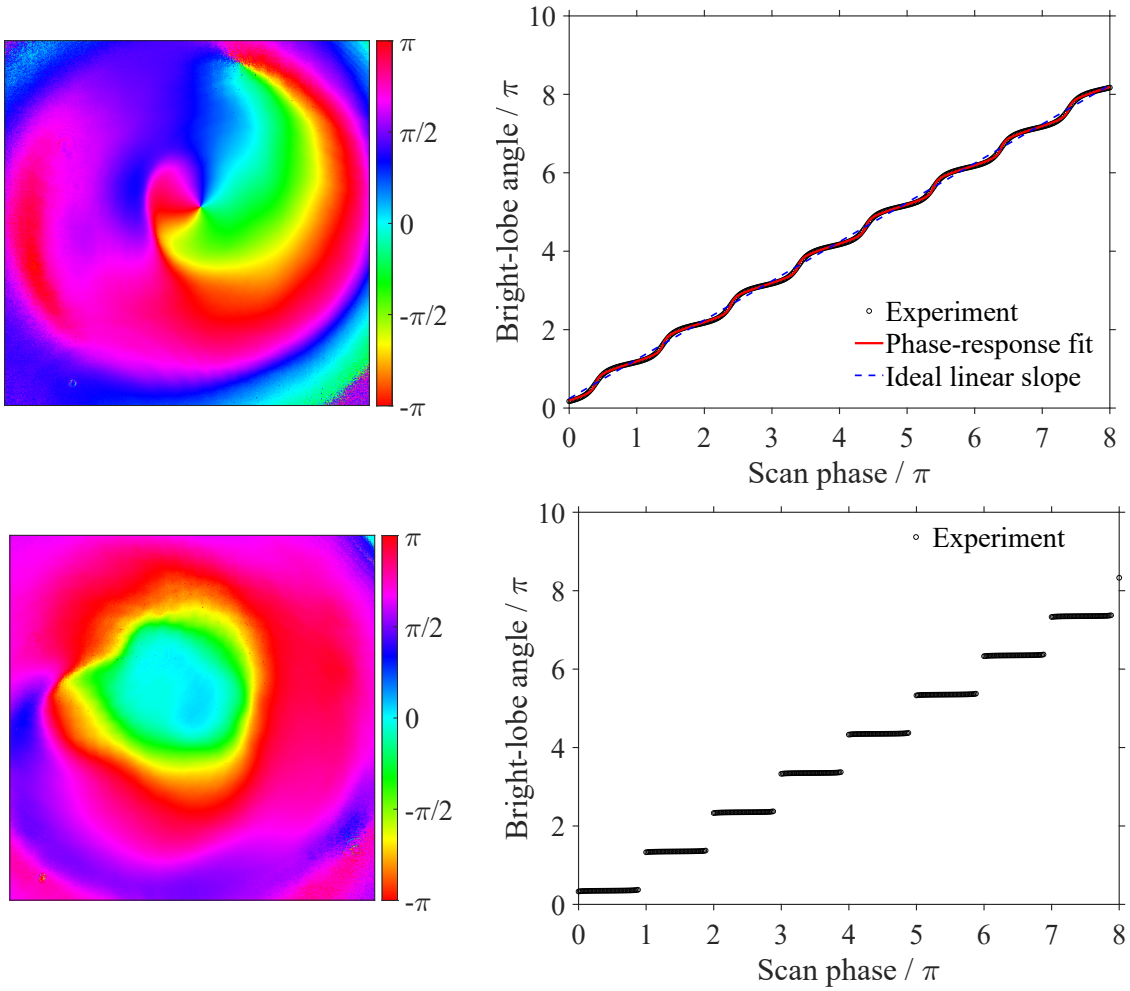
Equation (10) shows that displacing the analysing-pump singularity produces a nonuniform azimuthal phase gradient, rather than merely introducing a spatially uniform phase offset. This nonuniform gradient gives rise to the periodic deviation of the bright-lobe trajectory from the ideal linear response. The net relative-phase winding measured along a signal-centred circular contour C_ρ of radius ρ is

$$q_{\mathrm{rel}} = \frac{1}{2\pi}\oint_{C_\rho} d\delta_{\mathrm{rel}} = \ell - \ell_a\Theta(\rho - d), \tag{11}$$

where Θ is the Heaviside step function. The net relative-phase winding is therefore

$$q_{\mathrm{rel}} = \begin{cases} \ell - \ell_a, & d < \rho, \\ \ell, & d > \rho. \end{cases} \tag{12}$$

Thus, for equal winding numbers, $\ell_a = \ell$, the relative winding vanishes when the reconstruction contour encloses the analysing-pump singularity, whereas the intrinsic winding of the pair coherence is recovered when the singularity lies outside the contour.



S2. Effect of the pump singularity displacement on the phase-sensitive OPA response. Left: representative spatial phase distributions. Right: unwrapped bright-lobe angle as a function of the scanned phase. When the analysing-pump singularity lies outside the reconstruction contour ($d > \rho$), the intrinsic winding of the pair coherence is retained and the bright lobe rotates continuously; the experiment agrees with the displaced-singularity model in Eq. (13). When the singularity is enclosed by the contour ($d < \rho$), the pump and signal windings cancel for $\ell_a = \ell$, resulting in the staircase-like response.

For a globally scanned optical phase δ, the angular position of the bright lobe, φ_{B}, is determined by

$$\ell\varphi_{\mathrm{B}} + \varphi_0 - \ell_a \arg\Big(\rho e^{i\varphi_{\mathrm{B}}} - d\Big) = \delta + 2\pi m, \qquad m \in \mathbb{Z}. \tag{13}$$

For $d \gg \rho$, the azimuthal variation of the analysing-pump phase becomes weak, and Eq. (13) approaches

$$\varphi_{\mathrm{B}} \simeq \frac{\delta}{\ell} + \varphi_{\mathrm{off}}, \tag{14}$$

where φ_{off} is a constant angular offset.

For $d > \rho$, the nonzero relative winding gives rise to a continuously rotating bright lobe. At finite displacement, the nonuniform phase gradient of the analysing pump produces the small periodic modulation around the ideal linear trajectory. By contrast, for $d < \rho$ and $\ell_a = \ell$, the relative winding vanishes, producing the observed staircase-like response. In the concentric limit $d \to 0$, the relative phase becomes spatially uniform and the phase-dependent rotation disappears. The change from a staircase-like response to continuous rotation therefore indicates that the analysing-pump singularity has moved outside the signal reconstruction contour.

3. Spatial-mode selection in the two-BBO system

In the experiment, BBO1 generates multimode bright squeezed vacuum (BSV), whereas BBO2 acts as a phase-sensitive optical parametric amplifier (OPA). The spatial distribution measured after BBO2 is therefore determined by three processes: high-gain mode generation in BBO1, diffraction between the crystals, and mode-dependent amplification in BBO2. Together, these processes make the two-crystal system a coherent spatial-mode selector.

3.1 High-gain mode generation in BBO1

Under the undepleted-pump approximation, the spatial pair-coupling kernel of BBO1 is [5]

$$\Phi_1(\boldsymbol{q}_s, \boldsymbol{q}_i) = \mathcal{E}_{p,1}(\boldsymbol{q}_s + \boldsymbol{q}_i)\,\mathrm{sinc}\left(\frac{L_1\Delta k_{z,1}}{2}\right)\exp\left(i\frac{L_1\Delta k_{z,1}}{2}\right). \tag{15}$$

For a cylindrically symmetric interaction with a pump carrying OAM ℓ_p, angular-momentum conservation gives [6, 7]

$$\ell_s + \ell_i = \ell_p. \tag{16}$$

The Schmidt decomposition of the coupling kernel can be written as

$$\Phi_1(\boldsymbol{q}_s, \boldsymbol{q}_i) = \sum_{\ell_s,n} \sigma_{\ell_s,n} u_{\ell_s,n}(\boldsymbol{q}_s) v_{\ell_s,n}(\boldsymbol{q}_i), \tag{17}$$

where n labels the radial Schmidt modes and $\ell_i = \ell_p - \ell_s$. In the high-gain regime, the population of each mode pair is

$$N^{(1)}_{\ell_s,n} = \sinh^2(G_1\sigma_{\ell_s,n})\,, \tag{18}$$

with G_1 the overall gain of BBO1 [8]. The nonlinear dependence on $\sigma_{\ell_s,n}$ preferentially enhances the leading Schmidt modes, producing high-gain mode narrowing already in the first crystal.

3.2 Propagation and mode-dependent amplification in BBO2

During free-space propagation over the crystal separation D, each signal–idler mode pair acquires the paraxial phase

$$H_D(\boldsymbol{q}_s, \boldsymbol{q}_i) = \exp\left[-iD\left(\frac{|\boldsymbol{q}_s|^2}{2k_s} + \frac{|\boldsymbol{q}_i|^2}{2k_i}\right)\right]. \tag{19}$$

Propagation preserves the OAM indices in a cylindrically symmetric system, but changes the beam sizes, wavefront curvatures, and Gouy phases. Modes with larger radial or azimuthal orders generally diverge more strongly and therefore overlap less efficiently with the analysing pump in BBO2.

Because the phase singularity of the analysing pump is displaced by a distance d from the center of the reconstructed signal region, it lies outside the sampled region when $d > \rho$, where ρ is the reconstruction radius. If $\rho/d \ll 1$, the analysing field varies only weakly over this region and can be approximated locally as a zero-winding field,

$$\ell_a \simeq 0. \tag{20}$$

This approximation refers only to the local field sampled by the signal; the analysing pump may still carry a nonzero global topological charge. Accordingly, BBO2 is treated as selectively amplifying the OAM modes generated in BBO1.

In the propagated Schmidt basis of BBO1, the coupling of each mode pair to BBO2 is characterized by the spatial overlap

$$\mathcal{O}^{(2)}_{\ell_s,n}(D,\boldsymbol{d}) = \int d^2\boldsymbol{q}_s\, d^2\boldsymbol{q}_i\, \left[\Phi_2^{(\boldsymbol{d})}(\boldsymbol{q}_s,\boldsymbol{q}_i)\right]^* H_D(\boldsymbol{q}_s,\boldsymbol{q}_i) u_{\ell_s,n}(\boldsymbol{q}_s) v_{\ell_s,n}(\boldsymbol{q}_i). \tag{21}$$

When coupling between different Schmidt modes is negligible, BBO2 preserves the modal indices established in BBO1 and amplifies each mode pair with an effective squeezing parameter

$$r^{(2)}_{\ell_s,n} \simeq G_2 \left|\mathcal{O}^{(2)}_{\ell_s,n}(D,\boldsymbol{d})\right|, \tag{22}$$

where G_2 is the overall gain of the analysing OPA. Modes with smaller divergence and better wavefront matching have a larger overlap and therefore experience stronger second-stage amplification.

3.3 Two-crystal high-gain output

If the Schmidt bases of the two crystals are approximately matched, each mode pair can be treated as an independent two-mode amplifier. For vacuum input and negligible intercrystal loss, its output population is

$$N^{(12)}_{\ell_s,n} = \left|\cosh r^{(2)}_{\ell_s,n} \sinh r^{(1)}_{\ell_s,n} + e^{i\Delta_{\ell_s,n}} \sinh r^{(2)}_{\ell_s,n} \cosh r^{(1)}_{\ell_s,n}\right|^2, \tag{23}$$

where $r^{(1)}_{\ell_s,n} = G_1\sigma_{\ell_s,n}$ and $\Delta_{\ell_s,n}$ is the relative parametric phase, including the phase accumulated between the crystals. Constructive values of $\Delta_{\ell_s,n}$ produce amplification, whereas destructive values produce deamplification.

The detected normalized modal distribution is therefore

$$P^{(12)}_{\ell_s,n} = \frac{N^{(12)}_{\ell_s,n}}{\sum\limits_{\ell'_s,n'} N^{(12)}_{\ell'_s,n'}}. \tag{24}$$

Thus, the measured distribution is not simply the SPDC spectrum generated in BBO1 or the squared spatial overlap with BBO2. It results from high-gain Schmidt-mode selection in BBO1, propagation-dependent mode matching, and phase-sensitive amplification in BBO2. This combined mechanism preferentially selects the least-divergent modes with the best overlap with the analysing pump.

References

[1] Caves, C. M. & Schumaker, B. L. New formalism for two-photon quantum optics. i. quadrature phases and squeezed states. *Physical Review A* **31**, 3068–3092 (1985).

[2] Yurke, B., McCall, S. L. & Klauder, J. R. SU(2) and SU(1,1) interferometers. *Physical Review A* **33**, 4033–4054 (1986).

[3] Mandel, L. & Wolf, E. *Optical Coherence and Quantum Optics* (Cambridge University Press, Cambridge, 1995).

[4] Shen, Y. *et al.* Optical skyrmions and other topological quasiparticles of light. *Nature Photonics* **18**, 15–25 (2024).

[5] Law, C. K. & Eberly, J. H. Analysis and interpretation of high transverse entanglement in optical parametric down conversion. *Physical Review Letters* **92**, 127903 (2004).

[6] Mair, A., Vaziri, A., Weihs, G. & Zeilinger, A. Entanglement of the orbital angular momentum states of photons. *Nature* **412**, 313–316 (2001).

[7] Torres, J. P., Alexandrescu, A. & Torner, L. Quantum spiral bandwidth of entangled two-photon states. *Physical Review A* **68**, 050301 (2003).

[8] Sharapova, P. R., Pérez, A. M., Tikhonova, O. V. & Chekhova, M. V. Schmidt modes in the angular spectrum of bright squeezed vacuum. *Physical Review A* **91**, 043816 (2015).